Earth Planet. Sci. Lett. 642 (2024) 118835

Contents lists available at ScienceDirect

Earth and Planetary Science Letters

journal homepage: www.elsevier.com/locate/epsl

Enhanced mobility of granular avalanches with fractal particle size distributions: Insights from discrete element analyses

A.N. Shi [a], G.C. Yang [b], C.Y. Kwok [c,*], M.J. Jiang [d,a,e,**]

[a] Department of Civil Engineering, School of Civil Engineering, Tianjin University, Tianjin, 300072, Tianjin, China
[b] School of Aeronautics and Astronautics, Sun Yat-sen University, Guangzhou, 510275, Guangdong, China
[c] Department of Civil Engineering, The University of Hong Kong, Hong Kong, Haking Wong Building, Pokfulam Road, Hong Kong, China
[d] School of Civil Engineering, Suzhou University of Science and Technology, Suzhou, 215009, Jiangsu, China
[e] Shanghai Key Laboratory of Space Mapping and Remote Sensing for Planetary Exploration, Shanghai, 200092, Shanghai, China

ARTICLE INFO

Editor: J.P. Avouac

Dataset link: https://doi.org/10.6084/m9.figshare.21346398.v1

Keywords:
Granular avalanche
Fractal dimension
Flow mobility
Micro-mechanics

ABSTRACT

Granular avalanches are a form of hazardous landslide that rapidly travels long distances, with the grain-size distribution of their fragmented deposits developing fractal characteristics. In this study, we perform three-dimensional discrete element simulations of granular avalanches in a rotating drum to evaluate the effect of fractal particle size distributions on the flow mobility. The mobility of granular avalanches, measured as the inverse of the surface inclination angle, increases with the fractal dimension following a bilinear relationship with an abrupt slope change at a critical fractal dimension of 3.25, which delimits a roller-developing regime from a roller-active regime. The flow enters the roller-active regime when the fractal dimension is greater than 3.25, during which a complete basal layer of small particles separating the drum base and the flowing particles above is formed. Micro-mechanical evidence suggests that small particles at the drum base act as rotating bearings to reduce the effective basal friction, attenuate energy dissipation, and thereby enhance flow mobility.

1. Introduction

Geophysical flows, exemplified by rock avalanches, are characterized by their extremely rapid, massive, and flow-like motion of fragmented rock resulting from large rockslides (Hungr et al., 2014). These phenomena rank among the most hazardous geological events, posing significant risks to communities in mountainous areas (Melosh, 1990; Strom et al., 2019) and very costly in terms of human lives and engineering structures (Geertsema et al., 2006). Figs. 1(a) and 1(b) show two example of geophysical flows and their extremely long runout distance. These granular avalanches behave as rapid fluid flows during transport and emplacement, which is evidenced by their extreme mobility (up to tens of kilometers of runout distance) and greatly reduced dynamic friction (Kelfoun and Druitt, 2005; Crosta et al., 2007). Thus, many researchers have proposed hypotheses to explain this phenomenon, such as 'air-layer lubrication' (Shreve, 1968), 'fluidized-bed' (Kent, 1966), 'grain flow' (Hsu, 1975; Davies, 1982), 'acoustic fluidization' (Melosh, 1979), 'dynamic fragmentation' (Davies and McSaveney, 1999; Bowman et al., 2012) 'velocity-weakening' (Lucas et al., 2014), 'volume-weakening' (Aaron and Hungr, 2016; Legros, 2002) and so on. However, few of various inferences and conclusions have been confirmed or refuted.

Fragmentation or particle breakage occurs during transport due to inter-particle friction and collision (Davies and McSaveney, 2009; Langlois et al., 2015; Zhao et al., 2017, 2018), altering the particle-size distribution (PSD). The fragmentation of rock can lead to an impulsive force resulting in an additional fragment velocity to drive further runout for rock avalanches (Davies and McSaveney, 1999; Imre et al., 2010; Bowman et al., 2012; Haug et al., 2021). The deposit of a granular avalanche usually shows 'inverse grading', i.e., the local mean particle sizes fining from the upper surface to the base, and from the proximal to the distal end of granular avalanche deposits (Zhang and McSaveney, 2017), as shown in Fig. 1. The repeated fracture of particles results in a self-similar PSD which can be quantitatively characterized by the fractal dimension (D) using a power-law relationship $N(d) = N_0(d/d_0)^{-D}$, where $N(d)$ is the number of particles of diameter d, N_0 is the number of particles of a reference size d_0 (Hyslip and Vallejo, 1997). The mass fraction of smaller particles increases as the fractal dimension increases.

* Corresponding author.
** Corresponding author at: School of Civil Engineering, Suzhou University of Science and Technology, Suzhou, 215009, Jiangsu, China.
E-mail addresses: fkwok8@hku.hk (C.Y. Kwok), mingjing.jiang@tju.edu.cn (M.J. Jiang).

https://doi.org/10.1016/j.epsl.2024.118835
Received 10 August 2023; Received in revised form 17 April 2024; Accepted 4 June 2024

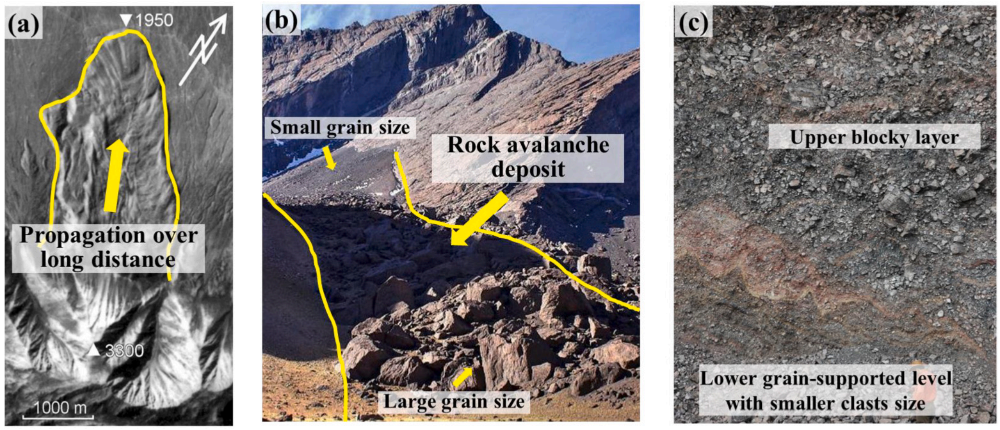

Fig. 1. Examples of historical granular avalanches. (a) The unconfined Chaartash - 3 rock avalanche (41.25°N, 74.0°E, Central TienShan, Kyrgyzstan). A fragment of the KFA - 1000 satellite image. Here and hereafter, numbers are elevations in meters above sea level of points marked by triangles. (modified from Strom et al. (2019)) (b) Cerro Tolosa rock avalanche in the Andes of central Chile and Argentina (modified from a photo by Martin Mergili, University of Graz). (c) Cross-section of a rock avalanche deposit showing a lower grain-supported level with smaller clasts size and a upper blocky layer (Crosta et al., 2017).

Various granular materials, such as artificially sheared sediment, ash, pumice, blasted rock, debris flow, ice fragments, and rock avalanches, have fractal dimensions ranging from 2.17 to 3.54 (Crosta et al., 2007).

It is well known that the coexistence of small and large particles in a polydisperse granular system has a significant influence on granular flow mobility (Phillips et al., 2006; Linares-Guerrero et al., 2007; Lai et al., 2017). Recently, the collapse of granular columns on a horizontal bottom plane has received much attention for the study of transient granular flows. Unlike immersed cases where complex fluid-particle interactions are non-negligible (Thompson and Huppert, 2007; Rondon et al., 2011; Jing et al., 2018, 2019; Yang et al., 2020, 2021), the dynamics of dry granular column collapses are mainly determined by the column geometry and the properties of granular materials (Balmforth and Kerswell, 2005; Lajeunesse et al., 2005; Lube et al., 2005). Granular column collapse experiments using *bidisperse* granular materials were conducted by Phillips et al. (2006) to examine the role of fine-material mass fraction on mobility in a transient flow. On one hand, small particles at the base can work as rotating bearings and lubricate the flow of coarse particles above. On the other hand, when the mass fraction of small particles is too high, the large number of contacts reduces the mobility of granular flows due to increased frictional losses. Linares-Guerrero et al. (2007) performed a similar study on bidisperse granular avalanches using two-dimensional (2D) numerical simulations based on the discrete element method (DEM) and confirmed the lubrication by a basal layer of small particles. Lai et al. (2017) performed 2D DEM simulations and experiments on the collapse of *polydisperse* granular materials following the fractal PSD and showed that the mobility of granular flows increased with fractal dimension. Meanwhile, Cabrera and Estrada (2021) conducted similar 2D DEM simulations and claimed that the fractal dimension had a minor effect on the granular flow mobility as long as the system was sufficiently large to avoid the grain-size effect (Cabrera and Estrada, 2019).

Therefore, it is still an ongoing debate about the role of fractal PSD and its relationship to granular flow mobility. The uncertainty can be partially attributed to the transient nature of granular column collapse, i.e., the flow dynamics vary both temporally and spatially, making the result sensitive to the specific configuration adopted in simulation and experiment. For example, a basal layer of small particles may form as a result of particle-size segregation (Jing et al., 2017; Möbius et al., 2001), and may not be fully developed during the short period of granular column collapse. This may restrict lubrication compared to a case where phase separation is dominant and covers almost the entire flow process, as commonly seen in natural landslides (Johnson et al., 2012; Kokelaar et al., 2014).

In this study, we investigate the effects of fractal PSD on the mobility of granular avalanches, when fragmentation and segregation are the two major processes, in a steady-state rotating drum configuration using a three-dimensional (3D) discrete element method. In contrast to the abovementioned granular column collapses, in which the runout distance and the flow duration are normally short due to the limited space, the setup of continuous granular flows in a rotating drum has been considered as an analogue experiment to long-runout landslides (Caballero et al., 2012, 2014; Yao et al., 2022). Here, we characterize the degree of segregation under the influence of fractal PSD. We aim to elucidate the role of small particles at the base from a micromechanical perspective, which is rarely discussed in experimental studies. Specifically, particle rotation versus sliding, the distribution of contact force networks, the effective friction coefficient between the drum base and the flowing particles, and the evolution of energy dissipation will be examined as the fractal dimension of the granular system is varied.

2. Model setup

In order to find the intrinsic mechanism of the influence of fractal PSD on the granular flow mobility, we used the Itasca software PFC3D (Particle Flow Code in three dimension), which is based on the discrete element method (Cundall and Strack, 1979), to run all the simulations presented herein. A linear spring-dashpot contact model was adopted. Fig. 2(a) presents the physical models in normal direction, which include a linear spring, a viscous damping dashpot and a divider. The normal contact force F_n is calculated as $F_n = F_n^l + F_n^d$, where $F_n^l = k_n\delta_n$ is the linear force in normal direction, δ_n is the normal overlap, k_n is the normal spring stiffness, $F_n^d = (2\beta_n\sqrt{m_c k_n})\dot{\delta}_n$ is the viscous dashpot force in normal direction, β_n is the normal damping ratio, $m_c = \frac{m^{(1)}m^{(2)}}{m^{(1)}+m^{(2)}}$ is the mass of body, $m^{(1)}$ and $m^{(2)}$ are the masses of two contacting particles, $\dot{\delta}_n$ is the relative normal translational velocity. In tangential direction (as shown in Fig. 2(b)), the physical models include a linear spring, a viscous damping dashpot and a slider. The tangential contact force F_s is calculated as $F_s = F_s^l + F_s^d$, where $F_s^l = (F_s^l)_0 + k_s\Delta\delta_s$ is the linear force in tangential direction, $(F_s^l)_0$ is the linear tangential force at the beginning of the timestep, $\Delta\delta_s$ is the relative tangential-displacement increment, k_s is the tangential spring stiffness, $F_s^d = (2\beta_s\sqrt{m_c k_s})\dot{\delta}_s$ is the viscous dashpot force in tangential direction, β_s is the tangential damping ratio, $\dot{\delta}_s$ is the relative tangential translational velocity. Then, the Mohr-Coulomb sliding criterion is used in the tangential direction, $F_s^\mu = \mu F_n^l$, where μ is the friction coefficient between two particles. The k_n and k_s are defined through the effective modulus E^* and the normal-to-shear stiffness ratio κ^*. The k_n is calculated as $k_n = A\kappa^*/L$,

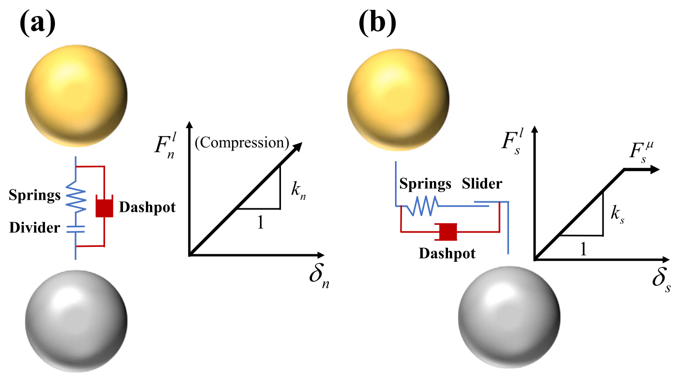

Fig. 2. Sketch of the linear spring-dashpot model between two interacting particles, as well as the force-displacement relationships along (a) the normal and (b) the tangential directions.

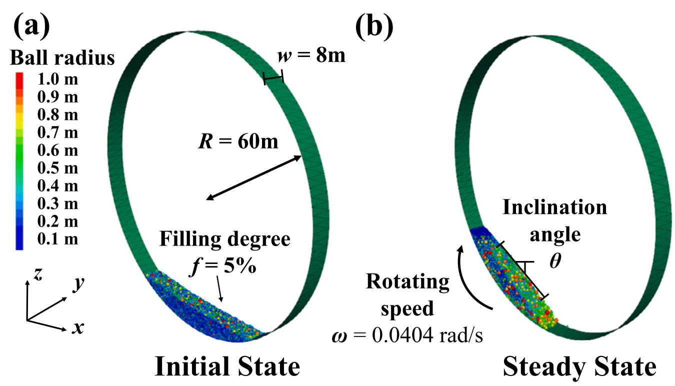

Fig. 3. Schematic diagram of a granular avalanche in a rotating drum. (a) Initial state, (b) Steady state.

where $A = \pi r^2$ is the contact sectional area, $r = \min(R^{(1)}, R^{(2)})$ is the minimum value of inter-particle radius, $L = R^{(1)} + R^{(2)}$ is the length of contact. The k_s is calculated as $k_s = k_n/\kappa^*$. For all simulations carried out in this study, a reduced effective modulus $E^* = 8$ MPa is adopted to increase the computational efficiency (Jing et al., 2019). Additional simulations with larger effective moduli, up to 800 MPa, have been conducted, revealing no significant impact on the numerical results (see Appendix A). Typical values for the κ^* and the inter-particle friction coefficient (μ) are adopted and are set to be 1.5 and 0.3, respectively. A relatively high value of damping ratio (0.8) is applied to represent the rough surface of real particles (Li et al., 2020) and to avoid highly agitated bouncing particles (Staron and Hinch, 2006). Simulations in this study were expanded to encompass lower damping ratios, down to 0.2, as detailed in Appendix B. Despite observing an effect of the damping ratio on the inclination angle, this influence does not modify the fundamental trend observed. This consistency serves to further validate the approach adopted in our simulations.

Fig. 3 illustrates the rotating drum setup with a radius (R) of 60 m and a width of 8 m. Periodic boundary conditions are defined in the y-direction to minimize the boundary effects. Additional simulations, extending drum widths and radii to 32 m and 100 m, respectively, reveal no significant impact on the numerical outcomes. To achieve dynamics similarity to large scale geophysical flows, a low filling degree of 5% is adopted such that the bed curvature effects are reduced (Schneider et al., 2011). According to Mellmann (2001), granular flows in a rotating drum can be classified into various regimes depending on a dimensionless Froude number, $Fr = \omega^2 R/g$, where ω is the rotation speed of the drum, and g is the gravitational acceleration (9.81 m/s^2). When the Froude number ranges from 10^{-4} to 10^{-2}, the particles inside the rotating drum flow continuously, which is associated with the so-called rolling regime. The major results presented in this study are obtained from simulations with a drum rotation speed of $\omega = 0.0404$ rad/s, corresponding to $Fr = 1 \times 10^{-2}$. Simulations in the rolling regime with smaller Froude numbers (i.e., 10^{-3} and 10^{-4}) have been performed and qualitatively similar results can be obtained. Time-averaged values between 3 and 5 revolutions of the drum are calculated, representing the steady-state granular flow behavior with small fluctuations.

The particles in our DEM simulations have ten different diameters evenly distributed from 0.2 m to 2 m. The total mass for each case is the same (6.79×10^6 kg). The number of particles of each size is determined by the PSD with the fractal dimension D ranging from 1.0 to 4.0, as shown in Fig. 4(a), which covers the range commonly seen in nature (Crosta et al., 2007). The PSD is also plotted as the percentage of the sample (by mass) that is smaller than a given particle size against a logarithmic scale of particle diameter, as presented in Fig. 4(b). One simulation with monodisperse particles and the diameter $d = d_{max} = 2$ m is conducted. It is regarded as the reference case, representing the condition in which no fragmentation occurs. It is well known that basal roughness plays an important role in the dynamics of granular flows and a sharp transition between slip and no-slip boundary conditions can be observed as the basal roughness gradually increases (Jing et al., 2016). In general, inter-particle collisions are enhanced by a higher basal friction coefficient, which promotes more frequent interchange of positions between particles with different sizes, resulting in an accelerated particle size segregation (Zhou et al., 2016). In this study, to ensure a fully segregated steady state can be achieved quickly, a high friction coefficient of 1.0 is adopted for the particle-wall interactions.

3. Results and discussion

3.1. Surface inclination angle

When the drum starts to rotate, the particles move upwards along the drum base until a maximum inclination angle θ of the free-surface is reached in the steady state, see Fig. 3(b). This inclination angle is commonly treated as a measurement of the frictional property of the granular material that defines the mobility (Chou et al., 2016). In general, the granular flow mobility increases as the inclination angle decreases. For example, a near zero inclination angle θ is expected when the granular material becomes totally frictionless in an extreme condition.

An interesting phenomenon observed in Fig. 5(a) is that the inclination angles of the cases with $D = 1.0$ and $D = 4.0$ are 21.5° and 28.1°, respectively. In fact, Fig. 5(b) shows that the inclination angle continuously decreases as the fractal dimension increases for the cases with different Froude numbers in the rolling regime. Compared to the inclination angle of the reference case with monodisperse particles when $Fr = 10^{-2}$, see the shaded area in Fig. 5(b), the inclination angle of the polydisperse cases is slightly affected by the PSD when the fractal dimension D is less than a critical value of 3.25. However, the reduction of inclination angle becomes significant when the fractal dimension D is greater than 3.25, and the other Froude number cases have the same tendency with the same critical value. The reduced inclination angle due to the increase of fractal dimension is a direct indication of an enhanced granular flow mobility accompanying fragmentation.

According to Cabrera and Estrada (2021), the shear strength of the bulk of the granular material is independent of the PSD. On the other hand, for spherical particles on a frictional base, shear is localized in the first layer of particles close to the base due to the rolling of the grains (Louge and Keast, 2001; Artoni et al., 2012). Also, small particles in polydisperse granular flows can gather at the base due to segregation and work as rotating bearings that lubricate the flow (Phillips et al., 2006; Linares-Guerrero et al., 2007; Lai et al., 2021). Therefore, we will focus on the micro-mechanical information of the particles and their interactions with the drum base to explain the reduction of inclination angle with the fractal dimension, especially when D is greater than 3.25.

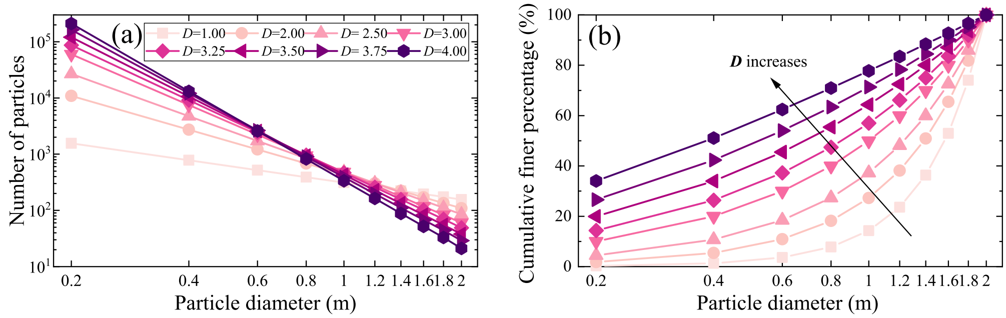

Fig. 4. Particle size distributions with different fractal dimensions D ranging from 1.0 to 4.0. (a) The number of particles against the particle size in a log-log plot. (b) The percentage passing by mass against the particle size in a linear-log plot.

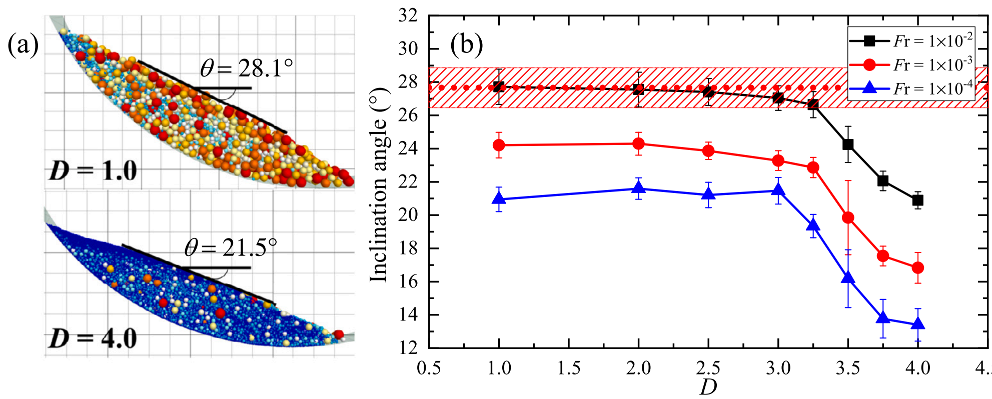

Fig. 5. (a) Comparing steady-state granular flows in a rotating drum with small ($D = 1.0$) and large ($D = 4.0$) fractal dimensions. Particles are painted according to the size and the color changes from blue to red as the size increases. (b) Plot of the time averaged surface inclination angle in the steady state against the fractal dimension for different Froude numbers. The error bars indicate the standard deviations due to time averaging, which also applies to the other figures. The shaded area indicates the variations of the inclination angle of the monodisperse case when $Fr = 10^{-2}$.

3.2. Formation of a basal layer of small particles

Due to particle size segregation, small particles percolate down through voids without enduring contacts and coarse particles climb up under shear (Möbius et al., 2001; Johnson et al., 2012; Thornton et al., 2012; Jing et al., 2017; Gray, 2018). Fig. 6(a) plots the number of the smallest particle at the base (N_s) against the fractal dimension D. When D is small, there are only a few smallest particles at the base and they concentrate at the tail of the flow, see the trajectories in the insets of Fig. 6(a). As D increases, the number of the smallest particle at the base also increases. Besides, the active flow region of the smallest particle gradually expands to the flow front. When D is 3.25, the smallest particles almost cover the whole basal layer and as D further increases, the number of the smallest particle at the base increases rapidly.

Following Linares-Guerrero et al. (2007), we use the Gini coefficient (G_s) to describe the distribution of the smallest particle at the base quantitively. The Gini coefficient is a measure of the inequality of a distribution defined by the Lorenz curve $L_s(x^*)$, $G_s = 2\int_0^1 L_s(x^*)dx^* - 1$, where x^* is the normalized base length with 0 and 1 corresponding to the tail and head of the flow, respectively. The Gini coefficient also varies between 0 and 1, representing perfect equality (well mixed state) and inequality (completely segregated state), respectively. The inset of Fig. 6(b) presents the Lorenze curves for the smallest particle at the base in initial and steady states when $D = 2.0$. Initially, particles are generated randomly inside the drum and then settle under gravity. As a result, the smallest particles are well-mixed and evenly distributed along the drum base, which is indicated by a nearly linear increase of the accumulative number of the smallest particle as x^* increases. When segregation fully develops in a steady state, the smallest particles translate to the tail of the flow, which is indicated by the sudden increase of the accumulative particle number when x^* is between 0 and 0.2.

The Gini coefficient G_s for the smallest particle in steady state is plotted against the fractal dimension D in Fig. 6(b), and a decreasing trend with a sudden change of rate at $D = 3.25$ is observed. A small Gini coefficient of 0.14 is obtained at $D = 4.0$, showing that the smallest particles are evenly distributed at the base. Combined with the large number of smallest particles at the base when D is large, we can conclude that a complete layer of fine particles separating the drum base and the flowing coarse particles gradually develops as the fractal dimension increases. Interestingly, the sudden change of behavior consistently at $D = 3.25$ reveals potentially a close relationship between the variations of the inclination angle and the formation of a basal layer of small particles.

3.3. Particle dynamics at the drum base

Fig. 7(a) plots the angular velocity of particles at the drum base against the particle diameter for different fractal dimensions. To achieve the same level of translational velocity at the contact point between the particles and the drum base, a higher angular velocity is observed for the smaller particles. Also, in our DEM simulations, the shear contact force is limited by the Coulomb friction, i.e., the product of the interparticle friction coefficient and the normal contact force, above which slippage will occur. Fig. 7(b) plots the percentage of slip contact with the drum base against the particle diameter for different fractal dimensions and it shows that large particles tend to slip more. In other words, small particles tend to stick to the base and rotate together with the drum quickly, similar to rotating bearings.

To find the micro-mechanical origin for the rolling motion of particles at the drum base, a confining force is calculated by summing up all the normal contact forces acting on a specific particle. This confining force is normalized by the total weight of the granular flow and is av-

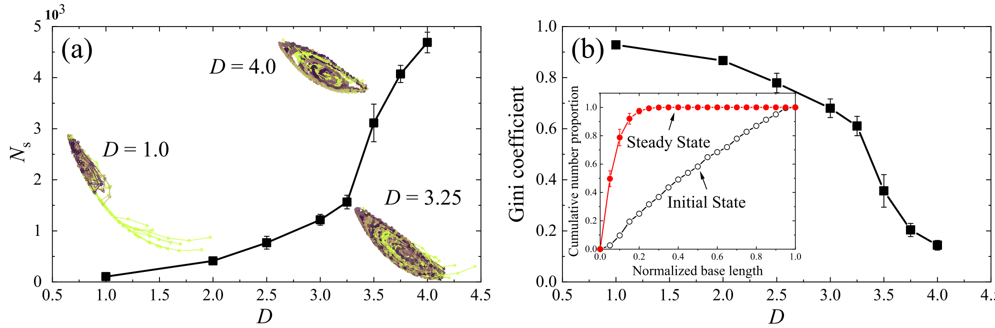

Fig. 6. (a) Plot of the number of the smallest particle ($d = 0.2$ m) at the base N_s against the fractal dimension. The insets illustrate the trajectories of the randomly selected smallest particles when $D = 1.0$, 3.25, and 4.0, with the color changing from light to dark when the particles move. (b) Plot of the Gini coefficient for the smallest particle at the base against the fractal dimension. The inset presents the Lorenz curves of the smallest particles at the base in initial and steady states when $D = 2.0$.

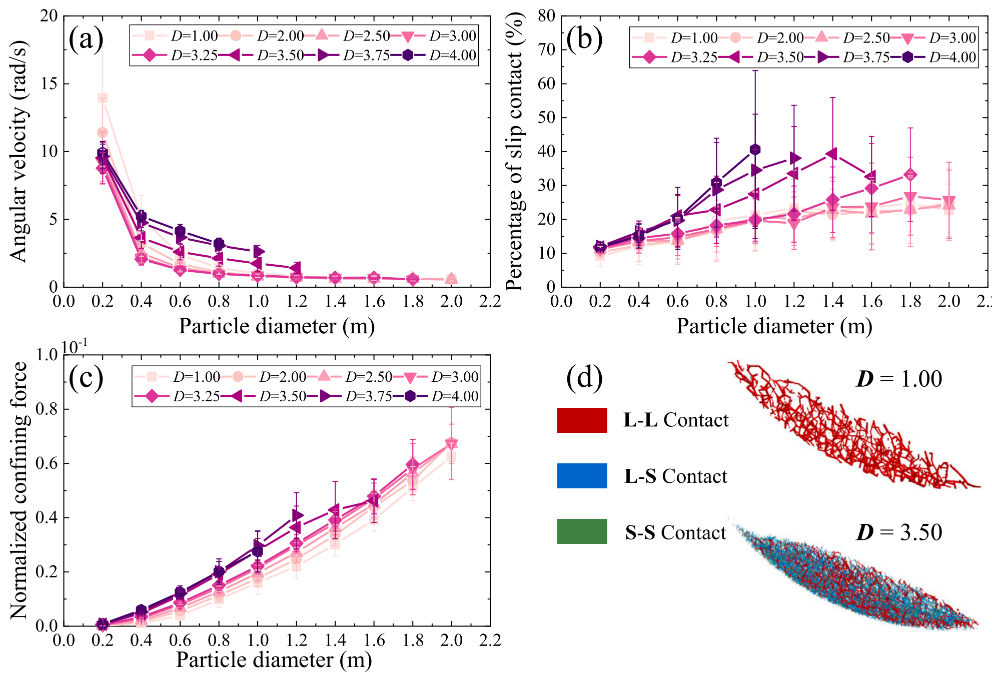

Fig. 7. Plot of (a) the angular velocity, (b) the percentage of slip contact at the base, and (c) the normalized confining force, against the particle diameter for different fractal dimensions. (d) Snapshots of the strong contact force network when $D = 1.0$ and $D = 3.5$. The red, blue, and green segments represent the contact between large-large (L-L), large-small (L-S), and small-small (S-S) particles, respectively. The thickness of the contact segments is proportional to the contact force magnitude.

eraged among a particular particle size, which is further plotted against the diameter in Fig. 7(c) for different fractal dimensions. It is found that the normalized confining force increases with the particle diameter significantly. Since the confining force should be positively correlated to the resistance to the rolling motion of particles under shear, small particles with a small confining force are free to roll and there are more restrictions to the rolling of larger particles under a larger confining force, which agrees with the results in Figs. 7(a) and 7(b).

Note that the large confining force acting on large particles is not just a result of more contacts with the surrounding particles. Fig. 7(d) shows the strong contact force networks at two different fractal dimensions (Radjai et al., 1998). When $D = 1.0$, most of the strong contact forces are supported by the large particles (mainly L-L contacts). When $D = 3.5$, the number of small particles increases significantly (see Fig. 4). Here, the small particles specifically refer to the particles with the minimum diameter $d = 0.2$ m. As a result, the number of L-S and S-S contacts also increases. Meanwhile, a high anisotropy of contact force magnitude is observed with the L-L contact segments much thicker than the others, indicating that the total weight of the granular flow is still mainly carried by the large particles when the fractal dimension increases. Therefore, the strong contact force chains going through the large particles lead to the large confinement that restricts the rolling motion. In contrast, the small particles rotate fast in between the strong contact force chains under less confinement, which is the kinematic origin for the lubrication of contacts between the drum base and the flowing particles.

3.4. Lubrication effect of small particles

To better characterize the lubrication effects of the small particles ($d = 0.2$ m) at the drum base, an effective friction coefficient μ_e is calculated by dividing the sum of the shear force by the normal force acting on the drum base. It is worth noting that the total shear force is determined by the shear component of the total contact force between the drum base and the particles, while the total normal force is derived from the normal component of the total contact force between the drum base and the particles. Fig. 8(a) shows that the effective friction coefficient μ_e decreases as the fractal dimension D increases. Similar to the evo-

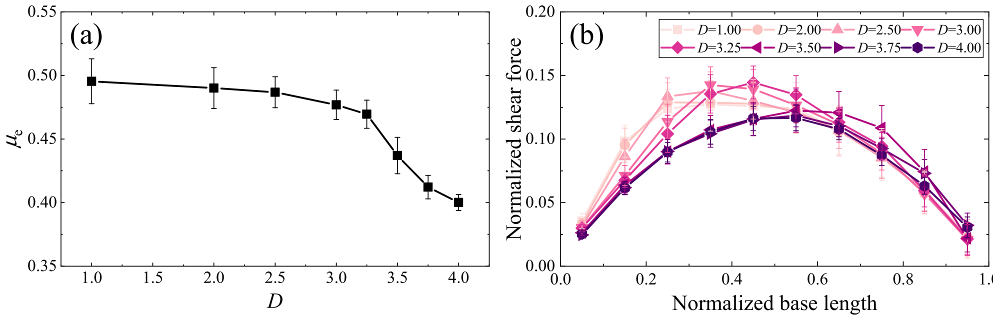

Fig. 8. (a) Plot of the effective friction coefficient μ_e at the drum base against the fractal dimension. (b) Spatial distributions of the shear force normalized by the total weight of the granular flow along the drum base for different fractal dimensions.

lution of the inclination angle, as shown in Fig. 5(b), there is a sudden change of rate at $D = 3.25$. More specifically, the effective friction coefficient μ_e decreases from 0.49 to 0.47 as D increases from 1.0 to 3.25, and quickly drops to 0.40 as D further increases to 4.0.

A more detailed examination of the spatial distributions of the normalized shear force along the drum base, as shown in Fig. 8(b), shows a close relationship between the friction coefficient reduction and the distribution of small particles at the base. The maximum shear force is found close to the center and gradually reduces as moving towards to the tail and front of the flow. When the fractal dimension is small, the small particles concentrate at the tail due to particle size segregation (see Fig. 6). In this case, the lubrication effect provided by the small particles at the base is limited. As the fractal dimension increases, the small particles gradually propagate to the middle of the flow where the shear force dominates. As a result, the position of the maximum shear force shifts towards the front of the flow, and the magnitude of the maximum shear force is reduced, indicating an enhanced lubrication effect provided by the small particles at the base.

According to MiDi (2004), the inertial number (I) is defined as a dimensionless quantity that weights the relative significance of inertia in comparison to confining stresses. The simulations reveal varying directions of local velocity gradients, reflecting the complex dynamics of the granular flow in rotating drum. Here, we focus on the data from a specific target region, which is defined by a plane with a width of 2.0 m perpendicular to the granular flow free surface and going through the drum center. This region is systematically divided into ten equal segments, spanning from the flow surface to the drum bottom. Fig. 9 shows the distribution of the time-averaged inertial number across the flow depth in steady state for various fractal dimensions. It is found that the inertial number almost decreases by two orders of magnitude as the fractal dimension D increases from 1.0 to 4.0. The small inertial number at high fractal dimension is mainly caused by the attenuated shear due to the lubrication effect. It is well known that the shear resistance of dense granular flows has a positive correlation with the inertial number. Therefore, the decrease of inertial number across the whole flow depth as D increases indicates that the lubrication at the base can induce a reduction in frictional resistance for the internal flow.

3.5. Total energy dissipation and flow regime transition

The reduced effective friction coefficient and shear force at large fractal dimensions, evidenced in Fig. 8, suggests that less energy is dissipated, which is associated with a high-mobility granular flow. However, the total energy dissipation due to friction and collision is generally difficult to access directly. Instead, the total energy dissipation is estimated as the work done by the rotating drum which is the product of shear force, rotation speed, and drum radius with the assumption that a balance between the input and output energy of the whole system is achieved in the steady state. The total energy dissipation per unit time is normalized by $\mu G \omega R$, where G is the total weight of the granular

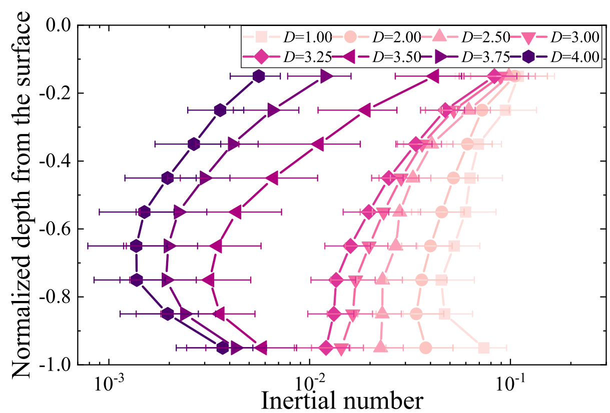

Fig. 9. Plot of the time-averaged inertial number from the flow surface to the drum bottom in steady state for various fractal dimension scenarios. Error bars represent the standard deviations arising from time averaging.

flow, and is plotted against the fractal dimension in Fig. 10. To examine whether our results can be generalized to other flow conditions, the results from cases with two different Froude numbers, i.e., $Fr = 10^{-3}$ and $Fr = 10^{-4}$, are also presented.

First, when $Fr = 10^{-2}$, the reference case with monodisperse particles has the most prominent energy dissipation compared to the polydisperse (as a representation of fragmentation) cases with various fractal dimensions. Second, there is less energy dissipation when the Froude number decreases, mainly due to the lower flow velocity. In addition, similar to the trend for the inclination angle as the fractal dimension increases, the total energy dissipation decreases only slightly when D is less than 3.25, and drops quickly when D is greater than 3.25, independent of the Froude number. It means that the sudden change of mobility at $D = 3.25$ is an intrinsic characteristic of the flow, with the material properties and model setup adopted in this study.

We can classify granular flows in a rotating drum into two different regimes: roller-developing regime and roller-active regime, according to the fractal dimension (indicated by the dotted line in Fig. 10). In the roller-developing regime, there is a limited number of small particles in the flow and they concentrate at the tail where the shear resistance is small, resulting in an insignificant lubrication effect. In the roller-active regime, a complete basal layer of small particles separating the drum base and the flowing particle above is formed, working as rotating bearings that lubricate the contacts significantly. As a result, the granular flow mobility is enhanced.

3.6. Discussion and limmitations

Recently, the high mobility fluid-like behavior of crushed rock avalanches was observed by Hu et al. (2022) from a series of high-speed rotary shear experiments. A sharp phase transition characterized by the

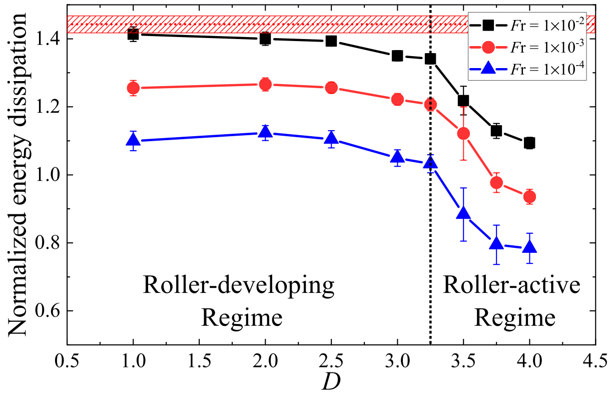

Fig. 10. Plot of the normalized total energy dissipation per unit time against the fractal dimension for cases with different Froude numbers. The shaded area indicates the variations of the normalized total energy dissipation per unit time of the monodisperse case when $Fr = 10^{-2}$. The dotted line depicts the boundary between the roller-developing and the roller-active regimes.

significantly reduced apparent fluid viscosity was found after continuous shearing. Such a strength weakening behavior was not present when uncrushable steel balls were used, suggesting an important role of fragmentation. Interestingly, we estimated the fractal dimension of the crushed rocks after shearing based on the particle size distribution data from Hu et al. (2022), the result is around 3.0, which is close to the critical fractal dimension for regime transition reported here. However, it should be noted that the phase transition reported by Hu et al. (2022) is likely a different phenomenon compared to the flow regime transition in this study. In the rotary shear experiments, the flow is mainly driven by the shear, resulting in insignificant segregation of small and large particles after fragmentation. Instead, the flow motion inside the rotating drum is mainly driven by the gravity and significant particle size segregation takes place. The experimental results from Hu et al. (2022) suggest that the PSD of granular materials may affect the frictional property of the bulk flow, which requires future particle based simulations to explain its micromechanical origin.

The rolling resistance coefficient (β) is a parameter influencing the degree of relative inter-particle rotation. Due to the analogous effects of the rolling resistance coefficient and particle shape on granular mechanics, larger β values of 0.1, 0.25, and 0.5 were chosen for additional simulations for fractal dimensions (D) of 1.0, 2.0, 3.0, 3.25, and 3.5.

Fig. 11 illustrates how the inclination angle varies with the fractal dimension for different rolling resistance coefficients (β = 0.0, 0.1, 0.25, and 0.5). It reveals an increase in inclination angle with rolling resistance, indicating that rolling resistance limits inter-particle rotation and bolsters shear strength. As β increases, the reduction in inclination angle diminishes for D values ≥ 3.25. This is attributed to the restriction of relative inter-particle and particle-wall rotations by rolling resistance, which diminishes the rotating speed of smaller grains at the base, thereby attenuating the lubrication effect. The specific mechanism of how particle shape and fine-grain lubrication effect interact to influence granular flow mobility remains unclear, a detailed analysis will be conducted in a follow-up study.

The rock avalanche deposits in different sub-facies and regions have different characteristics of fractal PSD, which means that the upper layer has the smaller value of D, and the bottom layer has the larger value of D. For instance, Dufresne et al. (2016) and Dufresne and Dunning (2017) find each facies produces a unique grain size distribution in two carbonate rock avalanche deposits (Tschirgant in Austria and Films in Switzerland), the value of D is about 2.2 to 2.4 in jigsaw-fractured face, about 2.58 in fragmented face, and about 2.58 to 2.7 in shear zone face, respectively. The above features are similar to our simulations with the fine particles gathering in the basal layer. This similar

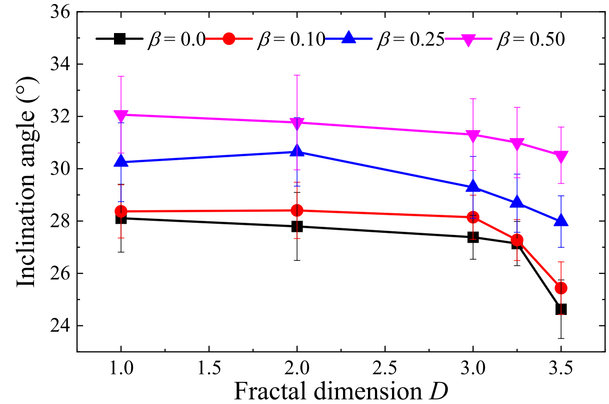

Fig. 11. Plot of the inclination angle against the fractal dimension D with the rolling resistance β = 0.0, 0.1, 0.25 and 0.5.

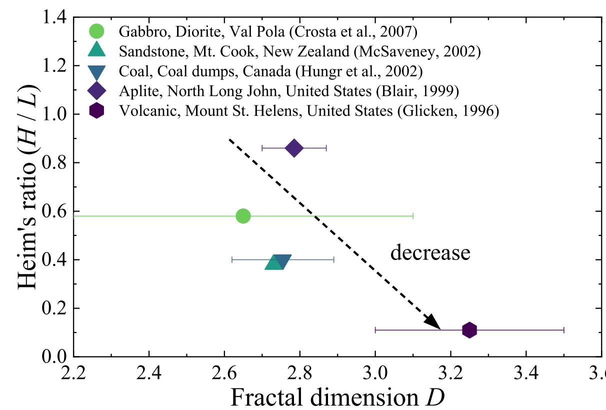

Fig. 12. Plot of the Heim's ratio H/L against the fractal dimension D with the deposits of rock avalanches in different regions (Crosta et al., 2007; McSaveney, 2002; Hungr et al., 2002; Blair, 1999; Glicken, 1996).

phenomenon indicates that our simulations have certain capabilities to capture the particle size distributions of rock avalanche deposits.

The diversity of PSD in rock avalanche deposits reflects variances in spatial location, fragmentation processes, and lithology. Due to the difficulty on data collection, only a few data on fractal dimension, lithology, and the Heim's ratio of H/L (ratio of fall height to horizontal travel distance) have been reported in literature. Fig. 12 shows that the deposits from different lithological contexts exhibit distinct fractal dimensions, which correlate positively in a certain extent with the lithological strength and fragmentation pressure. Despite the complex origins of rock avalanche deposits, a general trend emerges where the H to L ratio decreases with the fractal dimension. This trend is particularly pronounced in volcanic debris avalanches due to their inherent structural characteristics, which predispose them to more significant fragmentation compared to other rock types. This observation suggests a positive correlation between the flow mobility of rock avalanches and the fractal dimension, aligning with our simulation results.

4. Conclusions

To investigate the process when fragmentation is prominent in natural landslide events, such as rock avalanches, we simulate granular flows following different fractal particle size distributions in a rotating drum using 3D DEM. Different from previous studies on granular column collapses, a steady-state granular flow can be obtained in which particle size segregation is allowed to be fully developed. Our study provides micro-mechanical evidence to a hypothesis that small particles will sink to the base and lubricate the contacts similar to rotating bearings. It is due to the fact that the strong contact force chains mainly go through the large particles and restrict their rolling motion, allowing small particles in between to rotate freely, and thereby reduce the effective friction coefficient.

With the increase of the fractal dimension, the number of small particles increases and the lubrication becomes stronger, which enhances the overall granular flow mobility. This result is found to be valid in other flow conditions with different Froude numbers. However, the lubrication is significant only when the fractal dimension is large enough (greater than 3.25 in our rotating drum configuration) or the degree of fragmentation is high, which is required for the formation of a complete basal layer of small particles. As a result, granular flows in a rotating drum can be classified into a roller-developing regime (insignificant lubrication) and a roller-active regime (strong lubrication effect), depending on the fractal dimension.

Note that our study does not consider the dynamic disintegration process of fragmentation (Davies and McSaveney, 2009). Our results show that the change to the flow composition as a result of fragmentation can be a governing mechanism that causes the high velocity and long runout distance of large-volume landslides. This process is generally ignored in large-scale continuum simulations, and the micromechanical data presented in this study can be useful information for the development of constitutive models to access more accurate predictions and more economic design of countermeasures.

CRediT authorship contribution statement

A.N. Shi: Writing – original draft, Visualization, Methodology, Investigation, Formal analysis, Data curation. **G.C. Yang:** Writing – review & editing, Methodology, Investigation, Formal analysis, Data curation, Conceptualization. **C.Y. Kwok:** Writing – review & editing, Supervision, Methodology, Investigation, Formal analysis. **M.J. Jiang:** Conceptualization, Funding acquisition, Project administration, Resources, Supervision.

Declaration of competing interest

The authors declare that they have no known competing financial interests or personal relationships that could have appeared to influence the work reported in this paper.

Data availability

The facilities of Figureshare services were used to access all the data presented in this paper. All the data in this paper can be found in the following link: https://doi.org/10.6084/m9.figshare.21346398.v1.

Acknowledgements

This research was conducted under the support of the General Research Fund (GRF), No. 17205821 and No. 17205222, the NSFC Project, No. 42107154 and No. 51890911, the NSFC Innovation Research Group Project, No. 42221002, the Hainan Province Key Research and Development Project, No. ZDYF2021SHFZ264, the Guangdong Basic and Applied Basic Research Foundation Project, No. 2023A1515012881.

Appendix A. Influence of the effective modulus E^* on the inclination angle

The problems for overlap between particles are one of the classics in the discrete element method. Fig. A.1 shows the mean particle overlap as a function of fractal dimension, revealing that overlaps range from about 1.0 to 1.2% for cases with $Fr = 1 \times 10^{-2}$, in the steady state. The mean overlap abruptly drops to 1.0% for D values greater than 3.25. These values are considered acceptable for granular flow simulations.

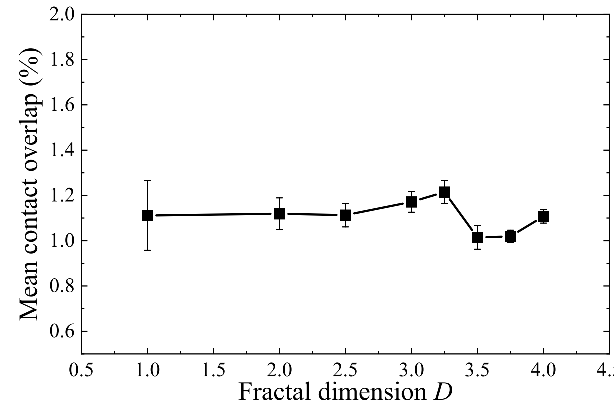

Fig. A.1. Plot of the mean contact overlap against the fractal dimension D.

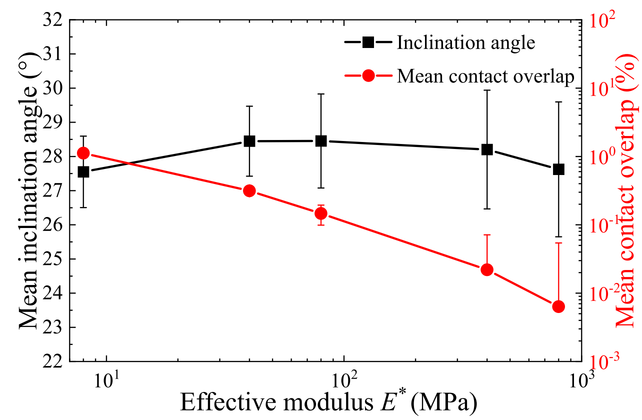

Fig. A.2. Plot of the mean inclination angle and the mean contact overlap against the effective modulus with the fractal dimension $D = 2.0$.

Additional simulation cases were conducted to explore the influence of E^* on flow mobility, with $E^* = 40$, 80, 400, and 800 MPa.

Fig. A.2 illustrates the relationship between the mean inclination angle and mean contact overlap with the effective modulus E^* for the case with $D = 2.0$. This figure demonstrates an almost linear decrease in mean contact overlap as E^* increases. Conversely, the mean inclination angle remains relatively stable, with minor variations around 28 degrees, across a broad E^* spectrum from 0.8 to 800 MPa. Notably, as E^* increases, the variation in inclination angle, as represented by the error bars, also enlarges because the particles closed to the free surface are more agitated. All in all, the effective modulus has a negligible influence on the inclination angle when $E^* \geq 8.0$ MPa. Thus, the use of a reduced $E^* = 8.0$ MPa will not alter our conclusions and save the simulation time significantly.

Appendix B. Influence of the viscous damping ratio on the inclination angle

To investigate the effects of damping ratio on granular flow mobility, simulations were conducted with damping ratios of 0.2, 0.5 and 0.8. Fig. B.3 depicts how the mean inclination angle varies with fractal dimension for different damping ratios. The data indicate that the inclination angle increases as the viscous damping ratio increases. All three cases with different damping ratios exhibit a similar trend: the inclination angle decreases with the increase fractal dimension. These findings indicate that while the damping ratio influences the inclination angle, the trend remains consistent across different damping ratios, highlighting the robustness of the relationship between the inclination angle and the fractal dimension.

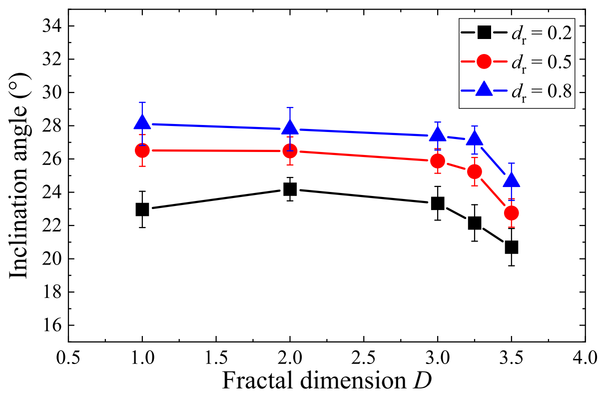

Fig. B.3. Plot of the mean inclination angle against the fractal dimension with the damping ratio $d_r = 0.2$, 0.5, and 0.8.

References

Aaron, J., Hungr, O., 2016. Dynamic analysis of an extraordinarily mobile rock avalanche in the northwest territories, Canada. Can. Geotech. J. 53, 899–908. https://doi.org/10.1139/cgj-2015-0371.

Artoni, R., Santomaso, A.C., Go', M., Canu, P., 2012. Scaling laws for the slip velocity in dense granular flows. Phys. Rev. Lett. 108, 238002. https://doi.org/10.1103/PhysRevLett.108.238002.

Balmforth, N.J., Kerswell, R.R., 2005. Granular collapse in two dimensions. J. Fluid Mech. 538, 399–428. https://doi.org/10.1017/S0022112005005537.

Blair, T.C., 1999. Form, facies, and depositional history of the North long John rock avalanche, owens valley, California. Can. J. Earth Sci. 36, 855–870. https://doi.org/10.1139/e99-024.

Bowman, E.T., Take, W.A., Rait, K.L., Hann, C., 2012. Physical models of rock avalanche spreading behaviour with dynamic fragmentation. Can. Geotech. J. 49, 460–476. https://doi.org/10.1139/t2012-007.

Caballero, L., Sarocchi, D., Borselli, L., Cárdenas, A.I., 2012. Particle interaction inside debris flows: evidence through experimental data and quantitative clast shape analysis. J. Volcanol. Geotherm. Res. 231–232, 12–23. https://doi.org/10.1016/j.jvolgeores.2012.04.007.

Caballero, L., Sarocchi, D., Soto, E., Borselli, L., 2014. Rheological changes induced by clast fragmentation in debris flows. J. Geophys. Res., Earth Surf. 119, 1800–1817. https://doi.org/10.1002/2013JF002942.

Cabrera, M., Estrada, N., 2019. Granular column collapse: analysis of grain-size effects. Phys. Rev. E 99, 012905. https://doi.org/10.1103/PhysRevE.99.012905.

Cabrera, M., Estrada, N., 2021. Is the grain size distribution a key parameter for explaining the long runout of granular avalanches? J. Geophys. Res., Solid Earth 126, e2021JB022589. https://doi.org/10.1029/2021JB022589.

Chou, S.H., Hu, H.J., Hsiau, S.S., 2016. Investigation of friction effect on granular dynamic behavior in a rotating drum. Adv. Powder Technol. 27, 1912–1921. https://doi.org/10.1016/j.apt.2016.06.022.

Crosta, G.B., Frattini, P., Fusi, N., 2007. Fragmentation in the Val Pola rock avalanche, Italian Alps. J. Geophys. Res., Earth Surf. 112. https://doi.org/10.1029/2005JF000455.

Crosta, G.B., Hermanns, R.L., Dehls, J., Lari, S., Sepulveda, S., 2017. Rock avalanches clusters along the northern Chile coastal scarp. Geomorphology 289, 27–43. https://doi.org/10.1016/j.geomorph.2016.11.024.

Cundall, P.A., Strack, O.D.L., 1979. A discrete numerical model for granular assemblies. Geotechnique 29, 47–65. https://doi.org/10.1680/geot.1979.29.1.47.

Davies, T.R., 1982. Spreading of rock avalanche debris by mechanical fluidization. Rock Mech. 15, 9–24. https://doi.org/10.1007/BF01239474.

Davies, T.R., McSaveney, M.J., 1999. Runout of dry granular avalanches. Can. Geotech. J. 36, 313–320. https://doi.org/10.1139/t98-108.

Davies, T.R., McSaveney, M.J., 2009. The role of rock fragmentation in the motion of large landslides. Eng. Geol. 109, 67–79. https://doi.org/10.1016/j.enggeo.2008.11.004.

Dufresne, A., Bösmeier, A., Prager, C., 2016. Sedimentology of rock avalanche deposits–case study and review. Earth-Sci. Rev. 163, 234–259. https://doi.org/10.1016/j.earscirev.2016.10.002.

Dufresne, A., Dunning, S., 2017. Process dependence of grain size distributions in rock avalanche deposits. Landslides 14, 1555–1563. https://doi.org/10.1007/s10346-017-0806-y.

Geertsema, M., Clague, J.J., Schwab, J.W., Evans, S.G., 2006. An overview of recent large catastrophic landslides in Northern British Columbia, Canada. Eng. Geol. 83, 120–143. https://doi.org/10.1016/j.enggeo.2005.06.028.

Glicken, H., 1996. Rockslide-debris avalanche of may 18, 1980, mount St. Helens volcano, Washington. U. S. Geol. Surv. Open File Rep. 1, 96–677, https://doi.org/10.3133/ofr96677.

Gray, J.M.N.T., 2018. Particle segregation in dense granular flows. Annu. Rev. Fluid Mech. 50, 407–433. https://doi.org/10.1146/annurev-fluid-122316-045201.

Haug, Ø.T., Rosenau, M., Rudolf, M., Leever, K., Oncken, O., 2021. Short communication: runout of rock avalanches limited by basal friction but controlled by fragmentation. Earth Surf. Dyn. 9, 665–672. https://doi.org/10.5194/esurf-9-665-2021.

Hsu, K.J., 1975. Catastrophic debris streams (sturzstroms) generated by rockfalls. Geol. Soc. Am. Bull. 86, 129–140. https://doi.org/10.1130/0016-7606(1975)86<129:CDSSGB>2.0.CO;2.

Hu, W., Xu, Q., McSaveney, M., Scaringi, G., Huang, R., Wang, G., Gou, H., Zheng, Y., 2022. Fluid-like behavior of crushed rock flows. J. Geophys. Res., Earth Surf. 127, e2021JF006523. https://doi.org/10.1029/2021JF006523.

Hungr, O., Dawson, R., Kent, A., Campbell, D., Morgenstern, N., 2002. Rapid flow slides of coal-mine waste in British Columbia, Canada.

Hungr, O., Leroueil, S., Picarelli, L., 2014. The varnes classification of landslide types, an update. Landslides 11, 167–194. https://doi.org/10.1007/s10346-013-0436-y.

Hyslip, J.P., Vallejo, L.E., 1997. Fractal analysis of the roughness and size distribution of granular materials. Eng. Geol. 48, 231–244. https://doi.org/10.1016/S0013-7952(97)00046-X.

Imre, B., Laue, J., Springman, S., 2010. Fractal fragmentation of rocks within sturzstroms: insight derived from physical experiments within the eth geotechnical drum centrifuge. Granul. Matter 12, 267–285. https://doi.org/10.1007/s10035-009-0163-1.

Jing, L., Kwok, C.Y., Leung, Y.F., 2017. Micromechanical origin of particle size segregation. Phys. Rev. Lett. 118, 118001. https://doi.org/10.1103/PhysRevLett.118.118001.

Jing, L., Kwok, C.Y., Leung, Y.F., Sobral, Y.D., 2016. Characterization of base roughness for granular chute flows. Phys. Rev. E 94, 052901. https://doi.org/10.1103/PhysRevE.94.052901.

Jing, L., Yang, G.C., Kwok, C.Y., Sobral, Y.D., 2018. Dynamics and scaling laws of underwater granular collapse with varying aspect ratios. Phys. Rev. E 98, 042901. https://doi.org/10.1103/PhysRevE.98.042901.

Jing, L., Yang, G.C., Kwok, C.Y., Sobral, Y.D., 2019. Flow regimes and dynamic similarity of immersed granular collapse: a CFD-DEM investigation. Powder Technol. 345, 532–543. https://doi.org/10.1016/j.powtec.2019.01.029.

Johnson, C.G., Kokelaar, B.P., Iverson, R.M., Logan, M., LaHusen, R.G., Gray, J.M.N.T., 2012. Grain-size segregation and levee formation in geophysical mass flows. J. Geophys. Res., Earth Surf. 117. https://doi.org/10.1029/2011jf002185.

Kelfoun, K., Druitt, T.H., 2005. Numerical modeling of the emplacement of socompa rock avalanche, Chile. J. Geophys. Res., Solid Earth 110. https://doi.org/10.1029/2005JB003758.

Kent, P.E., 1966. The transport mechanism in catastrophic rock falls. J. Geol. 74, 79–83. https://doi.org/10.1086/627142.

Kokelaar, B.P., Graham, R.L., Gray, J.M.N.T., Vallance, J.W., 2014. Fine-grained linings of leveed channels facilitate runout of granular flows. Earth Planet. Sci. Lett. 385, 172–180. https://doi.org/10.1016/j.epsl.2013.10.043.

Lai, Z., Chen, D., Jiang, E., Zhao, L., Vallejo, L.E., Zhou, W., 2021. Effect of fractal particle size distribution on the mobility of dry granular flows. AIP Adv. 11, 095113. https://doi.org/10.1063/5.0065051.

Lai, Z., Vallejo, L.E., Zhou, W., Ma, G., Espitia, J.M., Caicedo, B., Chang, X., 2017. Collapse of granular columns with fractal particle size distribution: implications for understanding the role of small particles in granular flows. Geophys. Res. Lett. 44, 12,181–12,189. https://doi.org/10.1002/2017gl075689.

Lajeunesse, E., Monnier, J.B., Homsy, G.M., 2005. Granular slumping on a horizontal surface. Phys. Fluids 17, 103302. https://doi.org/10.1063/1.2087687.

Langlois, V.J., Quiquerez, A., Allemand, P., 2015. Collapse of a two-dimensional brittle granular column: implications for understanding dynamic rock fragmentation in a landslide. J. Geophys. Res., Earth Surf. 120, 1866–1880. https://doi.org/10.1002/2014JF003330.

Legros, F., 2002. The mobility of long-runout landslides. Eng. Geol. 63, 301–331. https://doi.org/10.1016/S0013-7952(01)00090-4.

Li, X., Dong, M., Jiang, D., Li, S., Shang, Y., 2020. The effect of surface roughness on normal restitution coefficient, adhesion force and friction coefficient of the particle-wall collision. Powder Technol. 362, 17–25. https://doi.org/10.1016/j.powtec.2019.11.120.

Linares-Guerrero, E., Goujon, C., Zenit, R., 2007. Increased mobility of bidisperse granular avalanches. J. Fluid Mech. 593, 475–504. https://doi.org/10.1017/S0022112007008932.

Louge, M.Y., Keast, S.C., 2001. On dense granular flows down flat frictional inclines. Phys. Fluids 13, 1213–1233. https://doi.org/10.1063/1.1358870.

Lube, G., Huppert, H.E., Sparks, R.S.J., Freundt, A., 2005. Collapses of two-dimensional granular columns. Phys. Rev. E 72, 041301. https://doi.org/10.1103/PhysRevE.72.041301.

Lucas, A., Mangeney, A., Ampuero, J., 2014. Frictional velocity-weakening in landslides on Earth and on other planetary bodies. Nat. Commun. 5, 3417. https://doi.org/10.1038/ncomms4417.

McSaveney, M., 2002. Recent rockfalls and rock avalanches in Mount Cook National Park, New Zealand. https://doi.org/10.1130/REG15-p35.

Mellmann, J., 2001. The transverse motion of solids in rotating cylinders–forms of motion and transition behavior. Powder Technol. 118, 251–270. https://doi.org/10.1016/S0032-5910(00)00402-2.

Melosh, H.J., 1979. Acoustic fluidization: a new geologic process? J. Geophys. Res., Solid Earth 84, 7513–7520. https://doi.org/10.1029/JB084iB13p07513.

Melosh, H.J., 1990. Giant rock avalanches. Nature 348, 483–484. https://doi.org/10.1038/348483a0.

Möbius, M.E., Lauderdale, B.E., Nagel, S.R., Jaeger, H.M., 2001. Size separation of granular particles. Nature 414, 270. https://doi.org/10.1038/35104697.

Phillips, J.C., Hogg, A.J., Kerswell, R.R., Thomas, N.H., 2006. Enhanced mobility of granular mixtures of fine and coarse particles. Earth Planet. Sci. Lett. 246, 466–480. https://doi.org/10.1016/j.epsl.2006.04.007.

Radjai, F., Wolf, D.E., Jean, M., Moreau, J.J., 1998. Bimodal character of stress transmission in granular packings. Phys. Rev. Lett. 80, 61–64. https://doi.org/10.1103/PhysRevLett.80.61.

Rondon, L., Pouliquen, O., Aussillous, P., 2011. Granular collapse in a fluid: role of the initial volume fraction. Phys. Fluids 23, 073301. https://doi.org/10.1063/1.3594200.

Schneider, D., Kaitna, R., Dietrich, W.E., Hsu, L., Huggel, C., McArdell, B.W., 2011. Frictional behavior of granular gravel-ice mixtures in vertically rotating drum experiments and implications for rock-ice avalanches. Cold Reg. Sci. Technol. 69, 70–90. https://doi.org/10.1016/j.coldregions.2011.07.001.

Shreve, R.L., 1968. The Blackhawk Landslide, vol. 108. Geological Society of America.

Staron, L., Hinch, E.J., 2006. The spreading of a granular mass: role of grain properties and initial conditions. Granul. Matter 9, 205. https://doi.org/10.1007/s10035-006-0033-z.

Strom, A., Li, L., Lan, H., 2019. Rock avalanche mobility: optimal characterization and the effects of confinement. Landslides 16, 1437–1452. https://doi.org/10.1007/s10346-019-01181-z.

Thompson, E.L., Huppert, H.E., 2007. Granular column collapses: further experimental results. J. Fluid Mech. 575, 177–186. https://doi.org/10.1017/S0022112006004563.

Thornton, A., Weinhart, T., Luding, S., Bokhove, O., 2012. Modeling of particle size segregation: calibration using the discrete particle method. Int. J. Mod. Phys. C 23, 1240014. https://doi.org/10.1142/s0129183112400141.

Yang, G.C., Jing, L., Kwok, C.Y., Sobral, Y.D., 2020. Pore-scale simulation of immersed granular collapse: implications to submarine landslides. J. Geophys. Res., Earth Surf. 125, e2019JF005044. https://doi.org/10.1029/2019jf005044.

Yang, G.C., Jing, L., Kwok, C.Y., Sobral, Y.D., 2021. Size effects in underwater granular collapses: experiments and coupled lattice Boltzmann and discrete element method simulations. Phys. Rev. Fluids 6, 114302. https://doi.org/10.1103/PhysRevFluids.6.114302.

Yao, T., Yang, H., Lourenço, S.D.N., Baudet, B.A., Kwok, F.C.Y., 2022. Multi-scale particle morphology evolution in rotating drum tests: role of particle shape and pore fluid. Eng. Geol. 303, 106669. https://doi.org/10.1016/j.enggeo.2022.106669.

Zhang, M., McSaveney, M.J., 2017. Rock avalanche deposits store quantitative evidence on internal shear during runout. Geophys. Res. Lett. 44, 8814–8821. https://doi.org/10.1002/2017GL073774.

Zhao, T., Crosta, G.B., Dattola, G., Utili, S., 2018. Dynamic fragmentation of jointed rock blocks during rockslide-avalanches: insights from discrete element analyses. J. Geophys. Res., Solid Earth 123, 3250–3269. https://doi.org/10.1002/2017JB015210.

Zhao, T., Crosta, G.B., Utili, S., De Blasio, F.V., 2017. Investigation of rock fragmentation during rockfalls and rock avalanches via 3-D discrete element analyses. J. Geophys. Res., Earth Surf. 122, 678–695. https://doi.org/10.1002/2016JF004060.

Zhou, W., Lai, Z., Ma, G., Yang, L., Chen, Y., 2016. Effect of base roughness on size segregation in dry granular flows. Granul. Matter 18, 83. https://doi.org/10.1007/s10035-016-0680-7.